Available online at www.sciencedirect.com
ScienceDirect
Journal of Sound and Vibration 308 (2007) 392–404
JOURNAL OF SOUND AND VIBRATION
www.elsevier.com/locate/jsvi

Numerical bifurcation analysis of a friction-driven vibro-impact system

Andre D.L. Batako[a,*], Michael J. Lalor[a], Petri T. Piiroinen[b,**]

[a]*Liverpool John Moores University, General Engineering Research Institute, Byrom Street, Liverpool L3 3AF, UK*
[b]*Department of Mathematical Physics, National University of Ireland, Galway, University Road, Galway, Ireland*

Accepted 29 March 2007
The peer review of this article was organised by the Guest Editor
Available online 19 June 2007

Abstract

The dynamic response of a friction-driven vibro-impact system is presented. The system has two degrees-of-freedom with discontinuous nonlinear forces applied (dry friction and impact). This new self-exciting system tends to self-synchronisation with a potential industrial application in the field of percussive-rotary drilling. Friction-induced vibration is used as the source of excitation of impacts, which in turn influences the parameters of stick–slip motion. The friction force is defined as a nonlinear function of the drive velocity and allows for self-excitation. The dynamic coupling of vibro-impact action with the stick–slip process provides entirely new adaptive features important for practical application. The self-exciting process (stick–slip) depends on the mechanical properties of the medium interacting with the device.

In this paper, which is the initial stage of a series of investigations into the full dynamic response of the system for scientific and engineering interests, the dynamic behaviour of the system motion without impact is presented. The equations of motion are solved numerically and the analysis is focused on the effects that discontinuity induced bifurcations have on the system. Within the scope of the assumptions made, a bifurcation diagram provides a further understanding of the system dynamic behaviour. Self-excitation and self-synchronisation using a single drive has some advantages that can be exploited in oil drilling applications.

1. Introduction

Friction is the antagonistic force that exists between contact surfaces of two bodies in relative motion. It resists statically (static friction) forthcoming motion and dynamically opposes established motion in the system (dynamic friction). In mechanisms where two elements are rubbing against each other, dry friction can cause wear and self-sustained vibration. This may lead to stick–slip motion in mechanical systems. However, dry friction can also be used as a damping in vibration control.

In oil drilling, dry friction induces vibrations that cause failure of drill pipes, intensive bit wear and consequently the overall drilling cost increase. The vibration of drilling structures contains simultaneously

*Corresponding author. Tel.: +44 0 151 231 2516; fax: +44 0 151 298 2447.
**Also to be corresponded to.
E-mail addresses: A.D.Batako@livjm.ac.uk (A.D.L. Batako), petri.piiroinen@nuigalway.ie (P.T. Piiroinen).

0022-460X/$ - see front matter © 2007 Published by Elsevier Ltd.
doi:10.1016/j.jsv.2007.03.093

elements of axial, bending and torsional vibration. Kyllingstad and Halsey [1] studied the drill bit stick–slip motion. Jansen [2,3] investigated the dynamical behaviour of a drill string, such as stick–slip motion, whirling and impact on the borehole. Brett [4] studied the relationship between the torque and the velocity of the bit with similar vibration. Jansen et al. [5] developed an active damping system for self-excited torsional vibration for drill string. He noticed that when the bit impacts against the borehole the vibration ceases. Elsayed et al. [6] suggested that the coupled torsional and axial vibration is caused by a fluctuation in the phase angle between surface undulation and cutters.

Vibration has always been regarded as having a destructive effect on human beings, construction and mechanical systems. However, vibration is predominantly used in pile driving, road and construction equipment, tamping, hammer drills, in machining of very hard materials, and many other hand-held machines. Vibro-impact theory [7] has introduced a new generation of machines and technological processes that use the synergistic effect of multiple impacts as a fundamental principle of operation.

The model presented in this paper, which was originally proposed by Batako [8], combines three strongly nonlinear processes (friction, vibration and impact) into one single mechanism and uses a mathematical tool to coordinate the mutual interaction of these processes. The resulting characteristic of the system is a synchronised motion that has various engineering applications. Batako [8] proposed a model of a self-exciting system that uses friction induced stick–slip motion to generate an impact action. The system synchronises dynamically its oscillatory motion and impacting action to ensure the best use of driving energy. An initial study of the system is given in Refs. [7–11].

This paper will mainly focus on the effect that the non-smoothness of the dry friction has in the dynamic response of the system. Attention is drawn to a class of *discontinuity-induced bifurcations* (DIBs) that is sometimes referred to as *sliding bifurcations* [12]. A sliding bifurcation is characterised by local transition from slip to stick–slip motion (or vice versa) when one or more parameters of the system are varied. To locate the occurrence of the DIBs in the parameter space, a numerical simulation method [13] is used together with a continuation scheme [14] that deals with systems that include stick–slip motion.

The study of the system is portioned into three parts. In this paper, part I, the response of the system without impact is undertaken. In part II, the synchronised vibro-impact motion of the system will be studied. In part III, the combined dynamic response of the system and the drive will be investigated to provide a full dynamic performance and stability of the device.

The paper is organised as follows. In Section 2, the mechanical model of the original system that includes both impacts and friction is presented, followed by a presentation, in Section 3, of the equations of motion of the simplified model without any impacts. Section 4 gives a short presentation of some of the numerical techniques used for the numerical bifurcation analysis in Section 5 and for the system exploration in Section 6. Finally, Section 7 summarises this paper and takes a look into future research.

2. Mechanical model of the system

Fig. 1 illustrates the schematic model of a friction-driven vibro-impact system. The drive (1) moves with constant linear speed v. A body (2) with mass m_1 is driven over rough surface through spring (3) with stiffness k_1. A right-angled lever (5) carries a striker (4) at its upper end and rotates freely about the pin (7) mounted on the drive (1). The lower end of the lever is linked on the one side to the body (2) through a secondary spring (6)

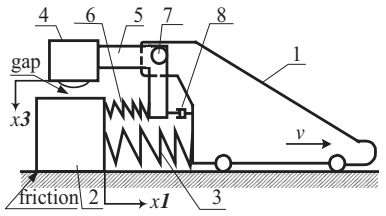

Fig. 1. A schematic picture of the friction-driven vibro-impact mechanical model, where 1 is the drive with constant velocity v; 2 is the body with mass m_1; 3 is the main spring with stiffness k_1; 4 is the striker with mass m_2; 5 is the lever; 6 is the secondary spring with stiffness k_2; 7 is the pin; 8 is the dashpot with viscous coefficient c_2.

with stiffness k_2. On the other side the lever is coupled to the drive by a dashpot with a viscous coefficient c_2. There is dry friction between the driven body (2) and the surface. It is assumed that the drive has a mass greatly exceeding the mass of the driven body (2) and is provided with unlimited power. Consequently, it is supposed that the motion of the drive is not affected by the dynamic response of the body (2).

The mechanism works as follows. The body (2) is driven over a surface by the drive (1) and due to dry friction between the contact surfaces the body can stick and slide intermittently. Consequently, spring (3) is compressed and extended alternatively. Such a stepwise motion causes a deformation of spring (6) that generates the oscillation of striker (4) around its equilibrium position. The body (2) and the striker (4) can vibrate at different frequencies, resulting in a complex non-periodical motion. This model is developed to exploit friction and stick–slip vibration to produce a periodic vibro-impact process where the body (2) and the striker (4) synchronise their motion.

The motion of the system begins with the body (2) being static. The drive (1) moves until the total force developed in the springs exceeds the static friction force at the interface between the body (2) and the surface. This motionless state is termed *sticking phase,* where a sticking phenomenon occurs between the body (2) and the surface. The drive keeps its motion constant and thus stretching spring (3). Because of the increasing distance between the drive (1) and body (2), the lever (5) rotates clockwise about the pin since its lower end is connected to body (2) through spring (6). Consequently, within the sticking phase the striker moves upwards. Lever (5) has a right angle between its upper and lower arm. The arms are of equal length and allow the lever to transform horizontal forces applied to the lower arm into vertical forces through its upper arm. By this means forces are transferred to the striker. At the instant when the total pulling force exceeds the static friction force, body (2) moves promptly following the drive. This phase of fast motion is called *slip phase*. With such a rapid motion, the body shifts the lever counter-clockwise through spring (6), pushing the striker towards the body (2). Collision between the striker and the body may occur depending on the amplitude of the oscillation. Within the slip phase, the force in spring (3) is released. However, a residual deformation of this element may occur depending on the position of the body (2) relative to the drive. At the end of the slip phase, the forces in the springs are reduced by relaxation. An additional braking effect takes place if an impact occurs. The static friction force becomes greater than total pulling force; the motion slows until the body (2) stops as the sticking takes place again. The cycle is repeated and such motion is known as *stick–slip motion*.

3. Mathematical model of the system

The equations of motion of the entire system as described in Section 2 have been studied in Refs. [7–11]. However, this paper is devoted to the study of some dynamical behaviour caused by bifurcations of the system motion without impacts. Consequently, the system is reduced to a two-degree-of-freedom oscillator with friction, as illustrated in Fig. 2(a), where the numbers have respective designation as in Fig. 1. An endless belt with a linear velocity v replaces the drive (1). The dry friction is applied in the robbing interface between the

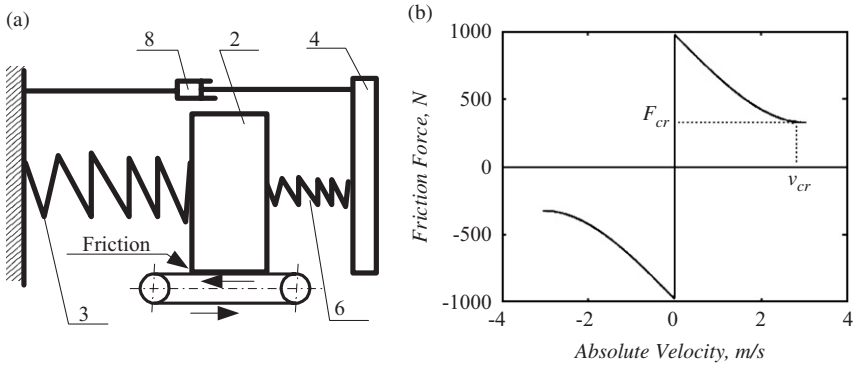

Fig. 2. (a) The mechanical system model without impact; (b) the friction force characteristics.

belt and the body (2) The friction force characteristic considered in this study is defined in Eq. (2) and is shown in Fig. 2(b).

The equations of motion for the mechanical system can be written as

$$\begin{aligned} m_1\ddot{x}_1 &= -k_1x_1 - k_2(x_1 - x_2) - F_r(y), \\ m_2\ddot{x}_2 &= -c_2\dot{x}_2 - k_2(x_2 - x_1), \end{aligned} \tag{1}$$

where $y = \dot{x}_1 + v$ is the relative velocity between body (2) and the belt with velocity v (see Fig. 2(a)).

There exist several ways to mathematically define a friction force that secures self-excitation properties. The structure in Fig. 1 is developed to model real engineering applications (e.g. drilling). Therefore in this study, the friction force F_r is defined as a function of the velocity, which is a real controllable parameter in engineering applications. The friction force is derived as

$$F_r(y) = \mu m_1 g\left(1 - \frac{|y|}{v_{\mathrm{cr}}} + \frac{|y^3|}{3v_{\mathrm{cr}}^3}\right)\mathrm{sgn}(y), \tag{2}$$

where μ is the friction coefficient and g the gravitational acceleration. In Fig. 2(b) and Eq. (2) v_{cr} is the critical relative velocity that defines the self-excitation properties of the system and $F_{\mathrm{cr}} = F_r(v_{\mathrm{cr}})$ is the corresponding friction force. The existence of self-sustained vibration is condition to $|v| < v_{\mathrm{cr}}$.

Dry friction has little effect on the system frequency response; consequently, the expression of friction force in Eq. (1) is neglected when finding the analytical solution of the system. However, due to the presence of dry friction, the system displays various dynamic responses depending on the relation between masses and stiffness and damping. The friction force is then expressed as

$$F_r(\dot{x}) = \begin{cases} \mu m_1 g\left(1 - \dfrac{|y|}{v_{cr}} + \dfrac{|y^3|}{3v_{cr}^3}\right)\mathrm{sgn}(y) \quad \text{for } y \neq 0, \\ \min\left[\left|k_1x_1 + k_2(x_1 - x_2)\right|,\ \mu m_1 g\right]\ \mathrm{sgn}(k_1x_1 + k_2(x_1 - x_2)) \quad \text{for } y = 0. \end{cases} \tag{3}$$

4. Numerical methods

The equations of motion (1) are solved numerically using a general simulation method [13] for systems that can employ stick–slip motion. In addition, different numerical analysis techniques are employed in the investigation of the system dynamic response caused by DIBs. In particular, the interaction of periodic orbits and the *discontinuity surface,* given by the function $y = 0$, where $y = \dot{x}_1 + v$, will be analysed. It is notable that the discontinuity surface gets its name because the friction force is set valued at this surface and the vector field, the right-hand side of Eq. (1), can be discontinuous across this surface.

Periodic orbits are located with a shooting method, which is based on Newton's method, with the introduction of a Poincaré surface. Since Newton's method requires the Jacobian of the corresponding Poincaré map, the fundamental solution matrix is obtained by solving the first variational equations corresponding to Eq. (1), where special care has been taken of the discontinuity in the vector field. See Ref. [15] for a detailed overview of this method. It is feasible to extend this method for continuation of periodic orbits under parameter changes. For instance, one can use Keller's pseudo-arclength method [16] to continue both limit-cycles in one parameter and discontinuity induced bifurcations in two parameters, see further Section 5.

Since the location and continuation methods use Jacobians of Poincaré maps for Newton's method it is also possible to get the linear stability of periodic orbits by finding the eigenvalues of the Jacobian corresponding to a limit cycle. A periodic orbit is linearly stable if all eigenvalues of the Jacobian lie within the unit circle of the complex plane. However, if at least one eigenvalue is outside the unit circle the limit cycle is unstable. Therefore, if at least one eigenvalues crosses the unit circle when a parameter is varied the system undergoes a bifurcation.

An equilibrium x^* for system (1) is found by setting the right hand side of the dynamical system corresponding to (1) equal to zero and solve for the state variables. The linear stability of the equilibrium is then determined by the eigenvalues of the corresponding Jacobian at $x = x^*$. The equilibrium is stable if the real parts of all eigenvalues are negative and unstable if one of the real parts is positive. On the other hand, a bifurcation (e.g. saddle-node, period-doubling or Hopf) occurs if one of the eigenvalues crosses the imaginary

axis, when a parameter is varied. In particular for Hopf bifurcations this idea makes it possible to find the parameter values for which the real parts of a complex conjugate pair of the eigenvalues lie on the imaginary axis. In Section 5, a secant method has been used to find a branch of Hopf bifurcations.

5. Analysis of system response—sliding bifurcations

Depending on the configuration of the parameters, the system displays various dynamical behaviours. The following parameter values were used to study the response of the system: $k_1 = 156{,}250\,\mathrm{N\,m^{-1}}$, $k_2 = 35156\,\mathrm{N\,m^{-1}}$, $m_1 = 250\,\mathrm{kg}$, $m_2 = 100\,\mathrm{kg}$, $c_2 = 250\,\mathrm{N\,s\,m^{-1}}$, $v_{cr} = 2.8\,\mathrm{m\,s^{-1}}$.

In Fig. 3, a two-parameter bifurcation diagram, in the friction parameter μ and the driving velocity v, is illustrated. This figure shows a branch of Hopf ('H') bifurcations of equilibria, sliding bifurcations (grazing–sliding ('GS') and switching–sliding ('SS')) of limit cycles. Recall that sliding bifurcations are here characterised by how transformation from stick to slip (or slip to stick) of limit cycles occurs, see further below. The two-parameter bifurcation diagram is divided into four separate areas where different dynamical characteristics are observed. A close look at the system response is undertaken at the points denoted by 'I', 'II', 'III' and 'IV'.

5.1. Area I

To the right of the Hopf curve 'H' in Fig. 3 the only attractors that are observed are equilibria. For high driving velocities the body (2) displays a transient response. This means that it approaches a constant position relative to the wall (see Fig. 2(a)), which is illustrated in Fig. 4, where body (2) displays a short transient response and comes back to the position of the equilibrium. The point 'I' in Fig. 5 denotes the equilibrium position of body (2) in the state space for this case. The system will display similar behaviour depending on the amount of damping and the relationship between masses and stiffness and the driving velocity. Note that the discontinuity surface corresponding to $y = 0$ is denoted by a dotted line in the relevant figures.

5.2. Area II

By decreasing the driving velocity v from point 'I' in Fig. 3, the system crosses the supercritical Hopf curve 'H' and move into the area of the point 'II'. Here stable limit cycles are observed, as shown in Fig. 5, where phase-space diagrams illustrate the limit cycle corresponding to the point 'II'. The corresponding time

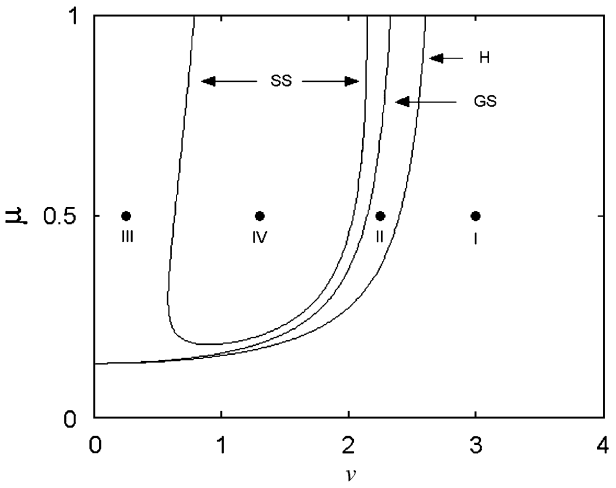

Fig. 3. A two-parameter bifurcation diagram (in belt velocity v and friction coefficient μ) showing branches of Hopf ('H'), grazing–sliding ('GS') and switching–sliding ('SS') bifurcations.

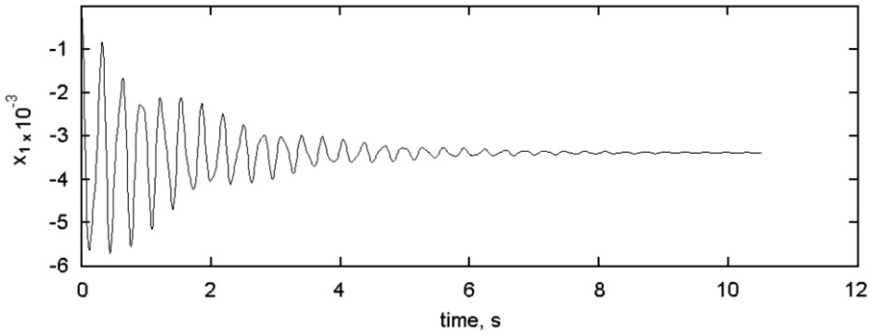

Fig. 4. A time plot of body (2) showing transient response and back to constant position.

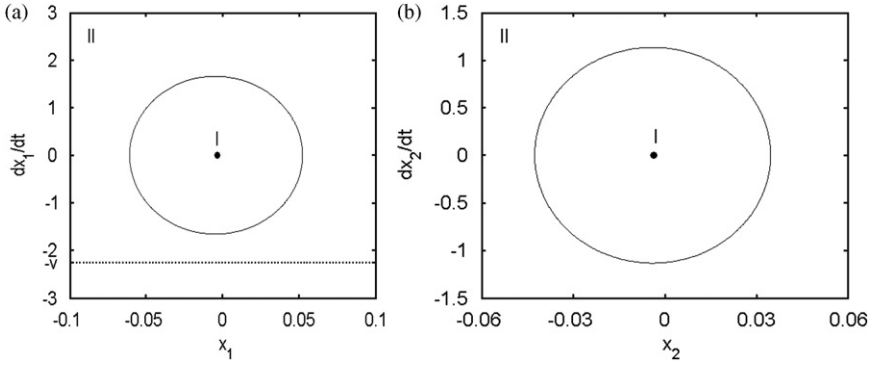

Fig. 5. Phase space diagrams for (a) dx_1/dt vs. x_1 and (b) dx_2/dt vs. x_2 of the attractors corresponding to the points 'I' and 'II' in Fig. 3. 'I' is an equilibrium and 'II' is a limit cycle. The dotted line in the left plot corresponds to the discontinuity surface.

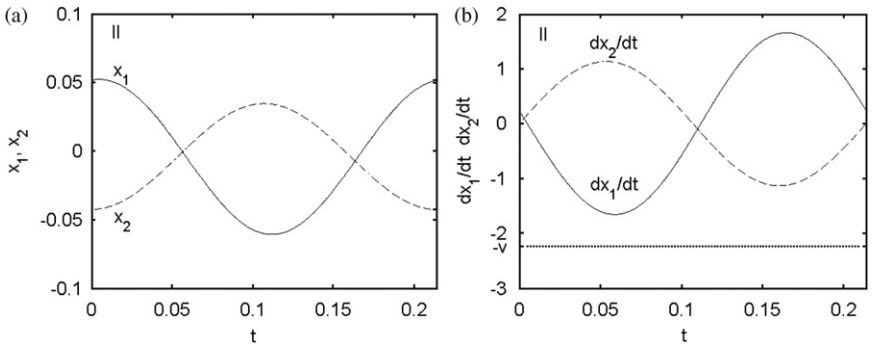

Fig. 6. Time histories for one period of the positions (a), x_1 and x_2, and the velocities (b), dx_1/dt and dx_2/dt, of the limit cycle corresponding to point 'II' in Fig. 3. The dotted line in the right plot corresponds to the discontinuity surface.

histories of the displacement and velocities for one period of the limit cycle are shown in Fig. 6. It can be noticed in Fig. 5(a) and in Fig. 6(b) that the limit cycle is relatively far away from the discontinuity surface. This means that the system is only performing slip motion.

5.3. Area III

A further decrease in the driving velocity will bring the system across the GS bifurcation curve ('GS' in Fig. 3), to the region of the parameter space denoted 'III'. On the actual branch 'GS' limit cycles graze the discontinuity surface, and by crossing the bifurcation curve the response of the system changes. The

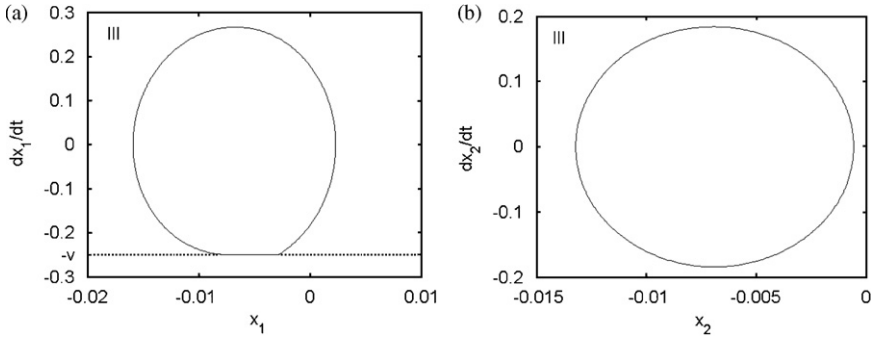

Fig. 7. Phase space diagrams, dx_1/dt vs. x_1 (a) and dx_2/dt vs. x_2 (b), of the limit cycle corresponding to the point 'III' in Fig. 3. The dotted line in the left plot corresponds to the discontinuity surface.

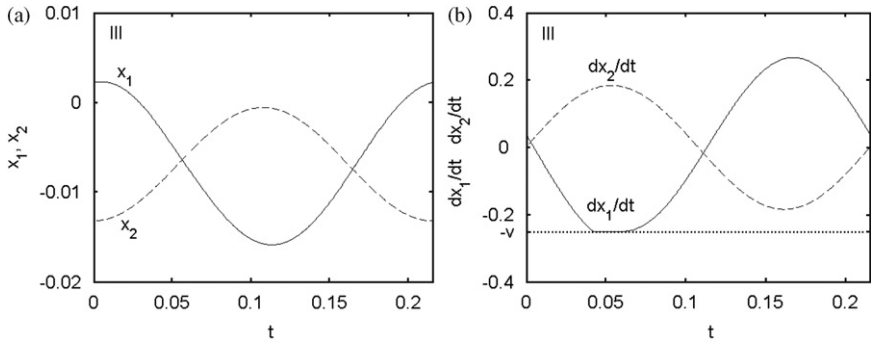

Fig. 8. Time histories for one period of the positions (a) x_1 and x_2, and the velocities (b) dx_1/dt and dx_2/dt, of the limit cycle corresponding to point 'III' in Fig. 3. The dotted line in the left plot corresponds to the discontinuity surface.

corresponding motion of the system is shown in Fig. 7, where the phase plot of the limit cycle displays a sticking phase. It can be seen in this figure that the body (2) enters the sticking phase for a period of time while the rest of the trajectory is in sliding phase. Consequently, in the region denoted 'III' the system always exhibits a "stick–slip" motion. Fig. 8 shows the corresponding time history of the displacements and the velocity profiles of both the body (2) and the striker.

Note that the Hopf bifurcation branch 'H' and the grazing bifurcation branch 'GS' in Fig. 3 come together tangentially as the driving velocity v decreases towards 0. This is because any decrease in the driving velocity v causes the discontinuity surface to move closer to the surface $dx_1/dt = 0$, which always must hold for equilibria. It also delimits the minimum amount of dry friction needed in the system in order to induce a self-excited and stable stick–slip motion depending on the system parameter configuration.

5.4. Area IV

In Fig. 3, it is observed that the SS bifurcation curve 'SS' forms a large area surrounded by the stable stick–slip zone. The response of the system in this area is depicted in Fig. 9(a), which corresponds to the point 'IV' in the bifurcation diagram. A particular aspect of this area is that close to the sticking phase a part of the trajectory crosses the discontinuity surface, as illustrated in Fig. 9(b). For our system this means that the body (2) moves faster than the belt for a short period of time, due to the release of the accumulated energy in the elastic element, before the short sticking phase.

6. Effect of mass and frequency ratio on system response

For further study of the system, the following proportionality factors are introduced: mass ratio $\beta = m_2/m_1$ and frequency ratio $\gamma = \omega_2/\omega_1$. Considering subsystems body (2) over spring 3 and striker 4 over spring 6 the

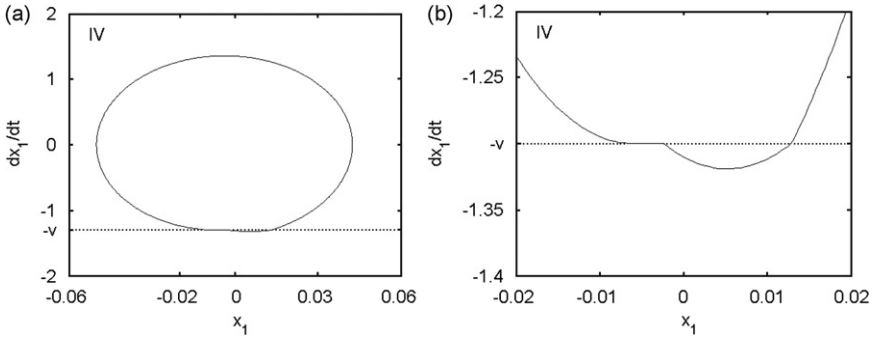

Fig. 9. Phase space diagrams, dx_1/dt vs. x_1 (a) of the limit cycle corresponding to the point 'IV', and close-look of the part of the limit-cycle (b) that interacts with the discontinuity surface. The dotted line in the left plot corresponds to the discontinuity surface.

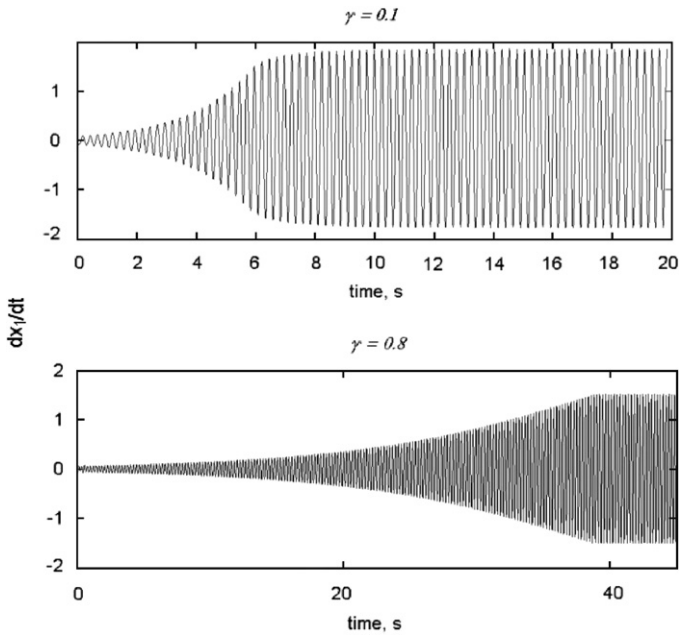

Fig. 10. System stabilisation time: $v = 1.5\,\mathrm{m\,s^{-1}}$; $\gamma = 0.1, 0.8$.

natural frequency of the body (2) and the striker is, respectively, $\omega_1 = (k_1/m_1)^{0.5}$ and $\omega_2 = (k_2/m_2)^{0.5}$. The study was undertaken for various system configurations by varying β and γ.

6.1. System settling stabilisation time

The time required from launch to the steady state motion (settling time) depends on the value of the driving velocity, the mass and the frequency ratio. Fig. 10 show the velocity of body (2) for different values of the frequency ratio γ when the driving velocity was set to $1.5\,\mathrm{m\,s^{-1}}$. These graphs illustrate the process of self-excitation and stabilisation. It is seen that the amplitude of oscillation increases gradually and reaches a steady state value for a stable motion and there is no further growth of the amplitude.

Fig. 11(a) shows the settling time of the system as a function of the driving velocity where it is observed that the settling time increases with the increase of the driving velocity. However, it is observed that in Fig. 11(b) the system settling time depicted as a function of the frequency ratio stays almost invariant up to $\gamma = 0.7$ where the settling time increases steeply. It was found in Refs. [9,11] in vibro-impact regime that the best optimum output of the system could be obtained around $\gamma = 0.7$ but not beyond this value and this graph supports this

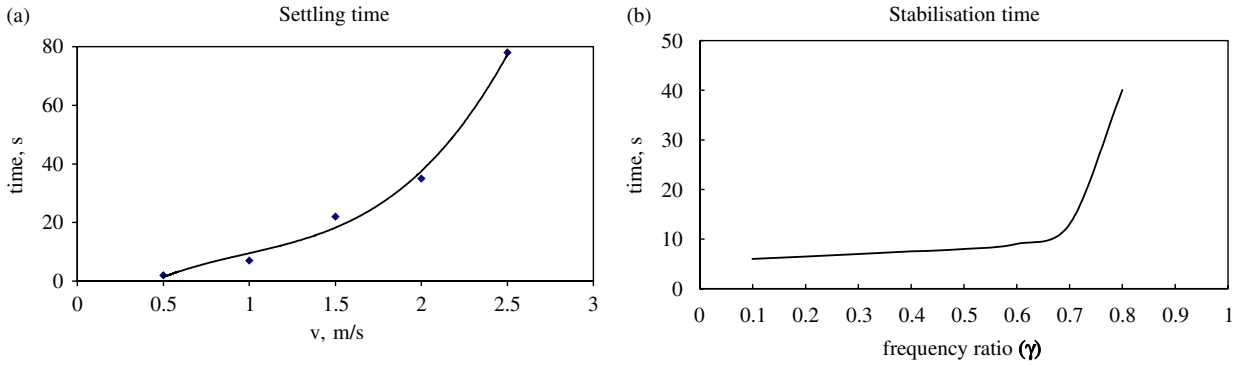

Fig. 11. Settling time as a function of velocity (a), and as a function of frequency ratio (b).

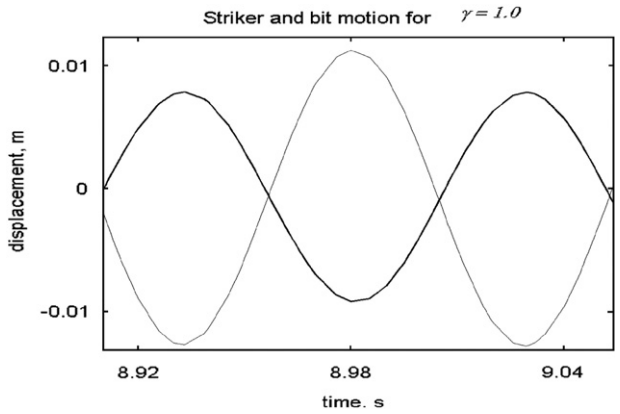

Fig. 12. Motion of body (2) and striker in clapping mode for $\beta = 0.3$ and $\gamma = 1.0$; thick line-x_1, thin line-x_2.

finding by showing that the settling time beyond 0.7 is very large and the system for some configuration may not reach a stable steady condition.

6.2. System response modes

It was observed that for some parameter configuration, both the body and the striker subsystems synchronise their motion and oscillate at a single frequency. In the vibro-impact regime it is important to secure maximum impact velocity therefore it is desirable to be able to define the mode in which the system operates. However, the obtained synchronised motion does not provide any information about the vibration mode. To identify the system response mode, the frequency ratio was varied while keeping a constant mass ratio.

The obtained results proved that it is possible to define the mode in which the system would vibrate. It was observed that for values of γ less than or equal to 1, the striker and the body (2) synchronise their motions but they move in counter phase as the second mode is excited. This is shown in Fig. 12 for $\beta = 0.3$ and $\gamma = 1.0$ where both the body (2) and the striker (4) are in a clapping mode (anti-phase) within a synchronized motion.

Equally Fig. 13 shows the response of the system for $\beta = 0.3$ and $\gamma = 1.2$, where the body (2) and the striker (4) oscillate in phase. It was found that for values of γ greater than 1.1, at the steady state synchronised motion, the striker and the body move in phase because the system switches back to its first mode of excitation. It is seen from this picture that the amplitude of both displacements are different.

6.3. System period doubling

The system also displays period-two motion for certain configuration of the parameters.

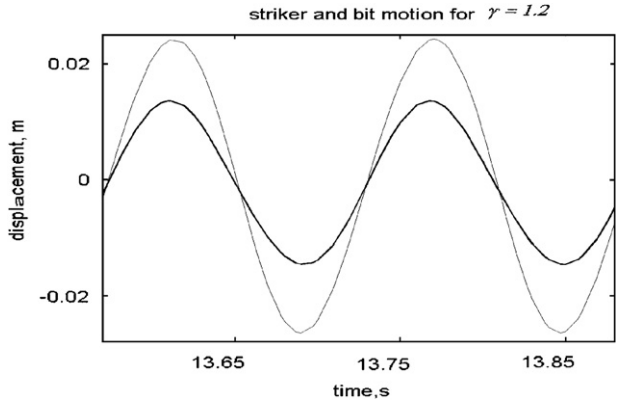

Fig. 13. Body (2) and striker (4) moving in phase for $\beta = 0.3$ and $\gamma = 1.2$; thick line-x_1, thin line-x_2.

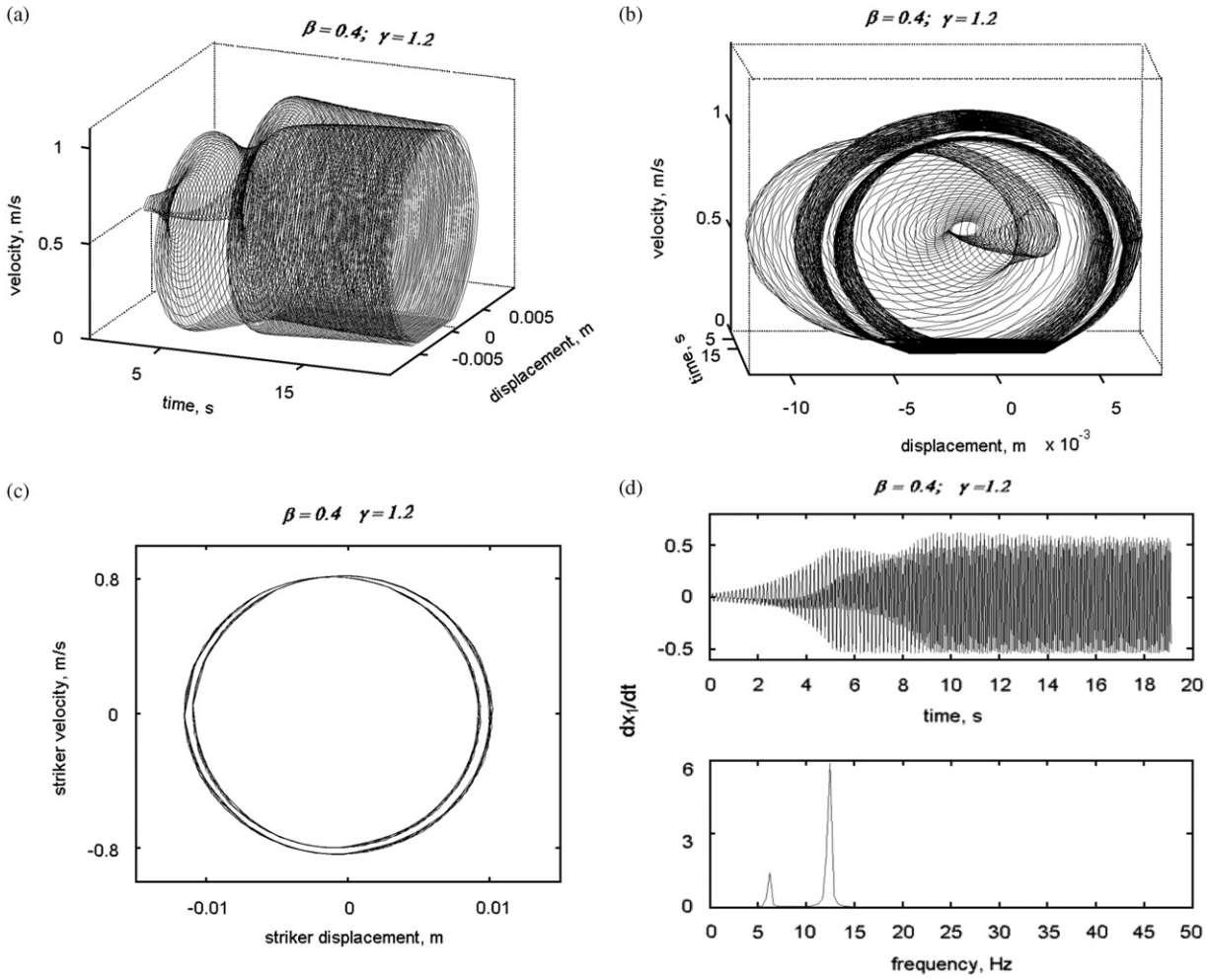

Fig. 14. System response for $\beta = 0.4$ and $\gamma = 1.2$; phase diagram (a, b) body (2) and striker (4) (c); frequency component (d).

Fig. 14(a) shows a 3D plot of a time-contained phase diagram of the body (2) motion, and Fig. 14(b) its clockwise rotation, for $\beta = 0.4$ and $\gamma = 1.2$. The onset of self-excitation with a period doubling is clearly observed. Fig. 14(c) illustrates the phase diagram for the striker (4) motion, which displays a period-two

motion. This is equally seen in Fig. 14(d) where the two frequency components are shown together with the time-based plot of the velocity. The two frequency components that system displays are 6.3 and 12.7 Hz. A further investigation is being undertaking to understand the aspects of period-doublings that the system may undergo.

6.4. *Effect of mass and frequency ratio*

In the design of vibro-impact systems the mass ratio is of great importance. It was noticed that in this system, the mass and frequency ratio have a strong influence on the system response. This paper only presents results from variation of frequency ratio while keeping mass ratio constant. Similar results but different in appearance can be obtained by varying the mass ratio whilst the frequency ratio is constant.

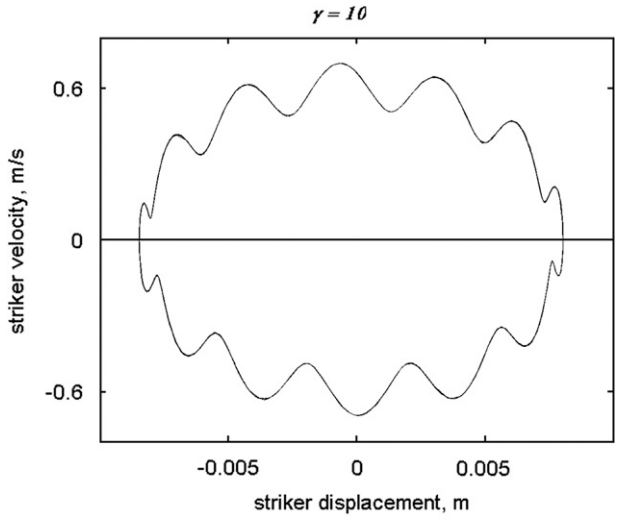

Fig. 15. Phase portrait of striker motion for $\beta = 0.3$ and $\gamma = 10$.

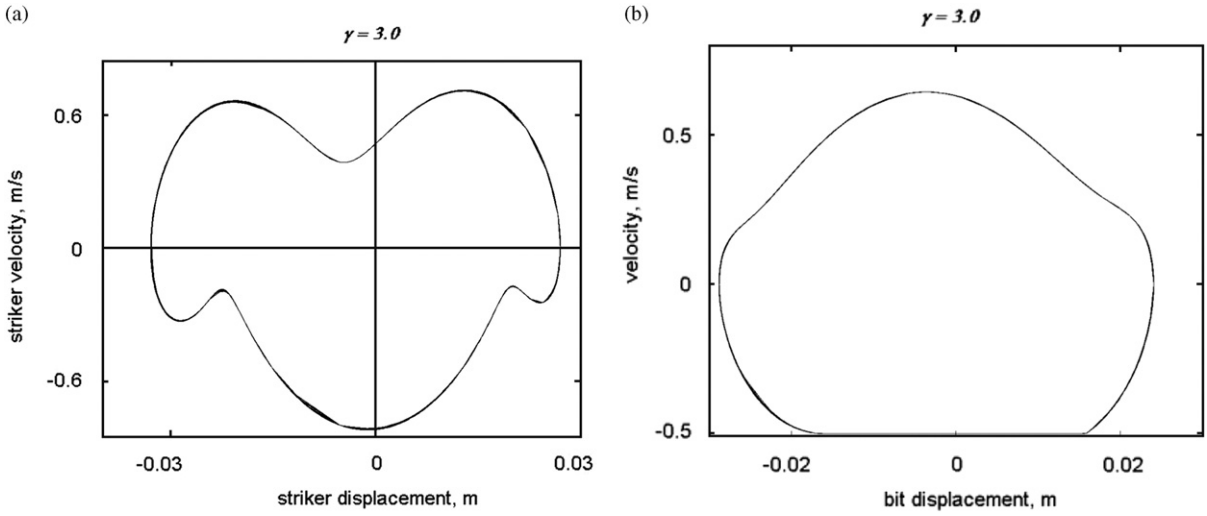

Fig. 16. Phase portrait of body (a) and striker (b) for $\beta = 0.3$ and $\gamma = 3$.

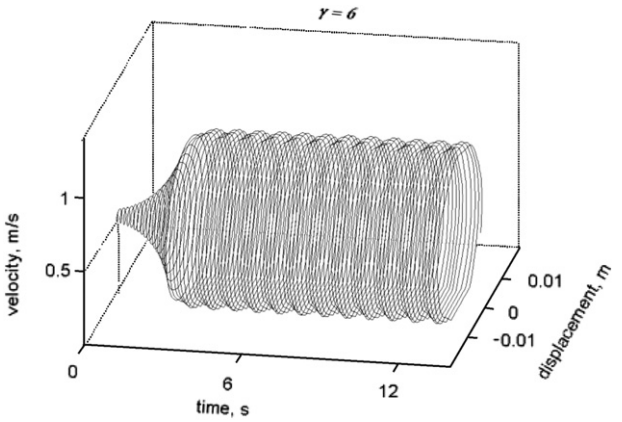

Fig. 17. Time contained phase diagram of body (2) motion for $\gamma = 6$; $v = 0.5\,\mathrm{m\,s^{-1}}$.

The result showed that for $2 \leqslant \gamma \leqslant 8$ the phase portrait of the striker motion displays lobes, and the number of lobes is equal to the integer part of γ. Furthermore, observations of the results revealed that if the integer part of γ is even, the lobes are spread symmetrically to the abscissa. This is illustrated in Fig. 15 by the motion of the striker for $\beta = 0.3$, $\gamma = 10$. The small lobes close to the abscissa are not considered as they appear constantly in all results. On the other hand, if the integer part of γ is an odd integer the lobes are not spread evenly. Fig. 16(a) shows the phase diagram of the motion of the striker for $\beta = 0.3$ and $\gamma = 3.0$, where three lobes are observed. The corresponding motion of the body (2) is shown in Fig. 16(b).

In addition, a kind of amplitude modulation is observed in the system response. This is illustrated in Fig. 17 for $\gamma = 6$ where the motion of the body (2) is modulated.

7. Conclusion

The mechanical system presented in this paper continues the study of the friction-driven vibro-impact system introduced in Refs. [7–11], where an extensive investigation of the system response under friction-induced vibration has been undertaken. The study in this paper was limited to the behaviour of the system without impact. Particular attention was paid to the bifurcation properties of the system caused by the discontinuous characteristic of the dry friction. The mathematical tools developed during this study allowed for obtaining a two-parameter bifurcation diagram that shows for what parameter values transitions between different stick–slip motions occurs for the system. The dynamics of the system in the different obtained areas in parameter space was also examined. In particular, the numerically obtained bifurcation diagram showed where in parameter space the systems is in sticking phase. For design purposes this is important since stick–slip motion is the backbone of the idea behind this vibro-impact system. The response of the system under various parameter configurations was also studied. It was shown that the mass and frequency ratio have an importance influence on the system behaviour. Elements of high-periodic motion were discovered for certain values of the system parameters. Further investigations are intended to undertake of these aspects in order to develop a full picture of the system response in this regime of motion. The results obtained are an invaluable asset towards the understanding of the system dynamical performance in vibro-impact mode.

Acknowledgement

Petri Piiroinen would like to express his thanks to the EU FP5 project SICONOS (Grant no. IST-2001-37172) for the financial support.

Andre Batako would like to thank the General Engineering Research Institute at Liverpool John Moores University for the support provided.

References

[1] A. Kyllingstad, G.W. Halsey, A study of slip–stick motion of the bit, *Society of Petroleum Engineers Drilling Engineering* 3 (1988) 369–373.
[2] J.D. Jansen, Non-linear rotor dynamics as applied to oil-well drillstring vibration, *Journal of Sound and Vibration* 147 (1991) 115–135.
[3] J.D. Jansen, Whirl and chaotic motion stabilized drill collars, *Society of Petroleum Engineers Drilling Engineering* 7 (1992) 107–114.
[4] G.F. Brett, The genesis of torsional drillstring vibration, *Society of Petroleum Engineers Drilling Engineering* 7 (1992) 168–174.
[5] J.D. Jansen, L. Van Den Steen, Active damping of self-excited torsional vibration in oil well drillstrings, *Journal of Sound and Vibration* 174 (4) (1995) 647–668.
[6] M.A. Elsayed, D.W. Dareing, M.A. Vonderheide, Effect of torsion on stability, dynamic forces, and vibration characteristics in drillstrings, *Journal of Energy Resources Technology—Transactions of the ASME* 119 (1997) 11–19.
[7] V.I. Babitsky, *Theory of Vibro-impact Systems and Applications*, Springer, Berlin, 1998 (Revised translation from Russian. Moscow: Nauka, 1978).
[8] A.D.L. Batako, A Self-exciting System for Percussive Rotary Drilling. PhD Thesis, Loughborough University, 2003.
[9] A.D. Batako, V.I. Babitsky, N.A. Halliwell, Self-oscillatory system of percussive-rotary drilling, *Journal of Sound and Vibration* 259 (1) (2003) 97–118.
[10] A.D. Batako, V.I. Babitsky, N.A. Halliwell, Modelling of vibro-impact penetration of self-exciting drill bit, *Journal of Sound and Vibration* 271 (2004) 209–225.
[11] A.D. Batako, Friction driven vibro-impact system with engineering applications, *Proceedings of EuroMech, ENOC-2005*, Eindhoven, Netherlands, 7–12 August 2005.
[12] Y.A. Kuznetsov, S. Rinaldi, A. Gragnani, One-parameter bifurcations in planar Filippov systems, *International Journal of Bifurcation and Chaos* 13 (2003) 2157–2188.
[13] P.T. Piiroinen, Yu.A. Kuznetsov, An event-driven method to simulate Filippov systems with accurate computing of sliding motion, *ACM Transactions of Mathematical Software* (2008), accepted for publication.
[14] P.T. Piiroinen, Numerical detection and continuation of sliding bifurcations in Filippov systems using an event-driven simulator, (2007), in preparation.
[15] H. Dankowicz, P.T. Piiroinen, Exploiting discontinuities for stabilization of recurrent motions, *Dynamical Systems* 17 (2002) 317–342.
[16] H.B. Keller, *Lectures on Numerical Methods in Bifurcation Problems*, Springer, Berlin, Heidelberg, New York, 1987.